DOI: 10.22184/FROs.2019.13.5.426.443

Hollow-Core Revolver Fibers (Properties, Design and Fabrication, Applications)

I. A. Bufetov, iabuf@fo.gpi.ru, A. F. Kosolapov, kaf@fo.gpi.ru, A. D. Pryamikov, pryamikov@fo.gpi.ru, A. V. Gladyshev, alexglad@fo.gpi.ru, A. N. Kolyadin, kolyadin@fo.gpi.ru, A. A. Krylov, krylov@fo.gpi.ru, Yu. P. Yatsenko, yuriya@fo.gpi.ru, A. S. Biryukov, biriukov@fo.gpi.ru
Fiber Optics Research Centre of RAS, www. fibopt.ru, Moscow

Hollow-core revolver fibers (RF) are a special type of hollow optical fibers with negative curvature of the core-cladding boundary. Their reflective cladding usually consists of a single layer of capillaries surrounding the hollow core. The physical mechanisms responsible for the waveguide properties of these fibers are discussed. A review of the optical properties and possible applications of hollow-core revolver fibers is given. Particular attention is paid to hydrogen Raman lasers of the mid-IR spectral range based on hollow-core revolver fibers and emitting in the range of 2.9–4.4 μm.

Key words: fiber optics, fiber design and fabrication, hollow-core fibers, Raman scattering

Received: 15.04.2019. Accepted: 06.05.2019.

Полые револьверные световоды (свойства, технология, применения)

И. А. Буфетов, iabuf@fo.gpi.ru, А. Ф. Косолапов, kaf@fo.gpi.ru, А. Д. Прямиков, pryamikov@fo.gpi.ru, А. В. Гладышев, alexglad@fo.gpi.ru, А. Н. Колядин, kolyadin@fo.gpi.ru, А. А. Крылов, krylov@fo.gpi.ru, Ю. П. Яценко, yuriya@fo.gpi.ru, А. С. Бирюков, biriukov@fo.gpi.ru
Научный центр волоконной оптики РАН, www. fibopt.ru, Москва

Полые револьверные световоды (РС) являются особым типом полых световодов с отрицательной кривизной границы сердцевина-оболочка. Их отражающая оболочка обычно состоит из одного слоя капилляров, окружающих сердцевину. Обсуждаются физические механизмы, ответственные за волноводные свойства данных световодов. Приведен обзор оптических свойств и возможных применений полых револьверных световодов. Особое внимание уделено водородным рамановским лазерам среднего ИК-диапазона, основанных на полых револьверных световодах, излучающих в диапазоне 2,9–4,4 мкм.

Ключевые слова: волоконная оптика, технология волоконных световодов, полые световоды, вынужденное комбинационное рассеяние (ВКР)

Статья получена: 15.04.2019. Принята к публикации: 06.05.2019.

1. INTRODUCTION

Revolver fibers (RF) is a new type of hollow-core optical fibers (HCF), which were first proposed and implemented in 2011 at the Fiber Optics Research Center of the Russian Academy of Sciences [1]. Cross-sections of hollow RFs, implemented to date, are presented in Fig. 1 (a - c). In [1], using the example of optical fibers of this type, the concept of optical fibers with a negative curvature of the core-cladding boundary was first introduced.

The analysis showed that this property (negative curvature) leads to a significant decrease in optical loss. Later on, fibers with negative curvature also referred to both to core fibers in the form of hypocycloid [2], and to light guides with a cladding consisting of elements similar to a stylized image of an ice cream cone or a parachute, developed later [3]. The main types of optical fibers with negative curvature of the cladding are shown in Fig. 1 (d). But RFs are significantly different from other fibers with negative curvature of the cladding due to the fact that, first, the cladding elements have cylindrical symmetry (more precisely, the cross-sectional shape of the elements is close to circular or elliptical) and, second, they can be placed around the core without contacting each other, which improves the fiber characteristics [4] (see Fig. 1 (a) and Fig. 1 (b)). Therefore, the authors proposed to refer to the optical fibers with a reflective cladding in the form of a single layer of cylindrical capillaries as to revolver fibers [5].

It should also be noted that in the publications relating to the RF, they were sometimes referred to as photonic-crystal fibers (PCF). Apparently, in this case, this term is inappropriate. Indeed, the waveguide properties in the PCF are due to the fact that they have a two-dimensional periodic structure in cross-section with a period of the order of the wavelength with the forbidden zones corresponding to the transparency zones of the optical fibers. In contrast to the PCF, the RF waveguide properties are mainly due to the reflection of radiation from structures at the core-cladding interface that do not have translational symmetry. The optical properties of the RF are determined by the material of the fiber, the geometric parameters of the cross-section of the fiber, and the stability of these parameters along the length of the fiber. The properties of the RF were studied by numerical methods in a significant number of researches (see, e.g., [9]).

This review is organized as follows: in the next section, the basic properties of the RF are considered using a simple analytical model; in Section 3, the properties of actual RF and the results of their numerical modeling are considered; Section 4 is dedicated to manufacturing technology of the revolver fibers. The use of the RF to create a hydrogen Raman laser of mid-IR range is considered in Section 5.

2. APPROXIMATE VISUAL DESCRIPTION OF THE RF'S LIGHT-GUIDING PROPERTIES

The RF's optical properties are determined by the optical properties of the material of which the fiber is made, and by the many geometric parameters of its cross-section, such as the diameter of the core, the shape and number of capillaries in the cladding, the diameter of the capillaries, their wall thickness, etc. As a result, the optical properties of RF can be obtained with sufficient accuracy only as a result of laborious numerical modeling (see, e.g., the recent extensive review [9] and references therein). In this section, however, an attempt is made to show that the main

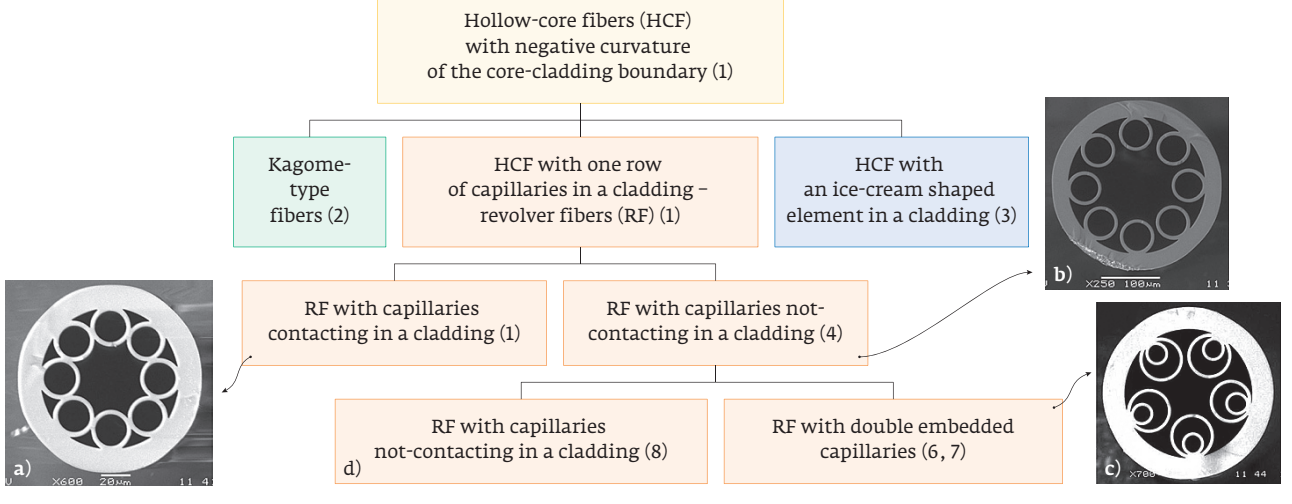

Fig. 1. *Photographs of transverse sections of revolver fibers: (a) RF with one row of contacting capillaries in a cladding [1] ; (b) RF with one row of non-contacting capillaries [4]; (c) RF with one row of double embedded capillaries [6], [7]; (d) a family of fibers with negative curvature of the core-cladding boundary*

waveguide properties of RF can be understood using some sort of successive approximation method.

As an initial approximation to the RF, the simplest model of an optical waveguide in the form of a hole in a dielectric (shown schematically in Fig. 2a) is taken. This hollow waveguide (HWG) was considered in detail in [10]. In this case, the Fresnel reflection from the surface separating the hollow core and the dielectric determines the level of optical losses of the fiber (Fig. 2d, black line). It is possible to significantly reduce the optical loss of the waveguide by increasing the reflection coefficient from the core-cladding interface, e.g., by arranging reflection from two surfaces, using a capillary with a thin glass wall (tubular waveguide, TWG) as a waveguide, and constructive interference of radiation reflected from both surfaces of the capillary. This type of fiber was considered in [11, 12], and it can be taken as a second approximation to the RF (TWG model). In this case, the capillary wall serves as a Fabry-Perot interferometer, and the transmission spectrum of the optical fiber accordingly acquires a band structure. When the resonance condition is satisfied for radiation incident on the wall with an angle of incidence close to $\pi/2$, the reflection coefficient decreases, which leads to large optical losses in the fiber. If the resonance condition is violated (or the antiresonance condition is satisfied), the reflection coefficient from the capillary wall increases significantly, and the transparency zones of the optical fiber are formed (see Fig. 2 (d), red line).

Later, the mechanism was actually reconsidered in [13] and was abbreviated as ARROW (AntiResonant Reflecting Optical Waveguide). Note that further improvement of the resonantly reflecting fiber cladding is possible (see, e.g., [14]), which in the case of RF leads to a structure with double embedded capil-

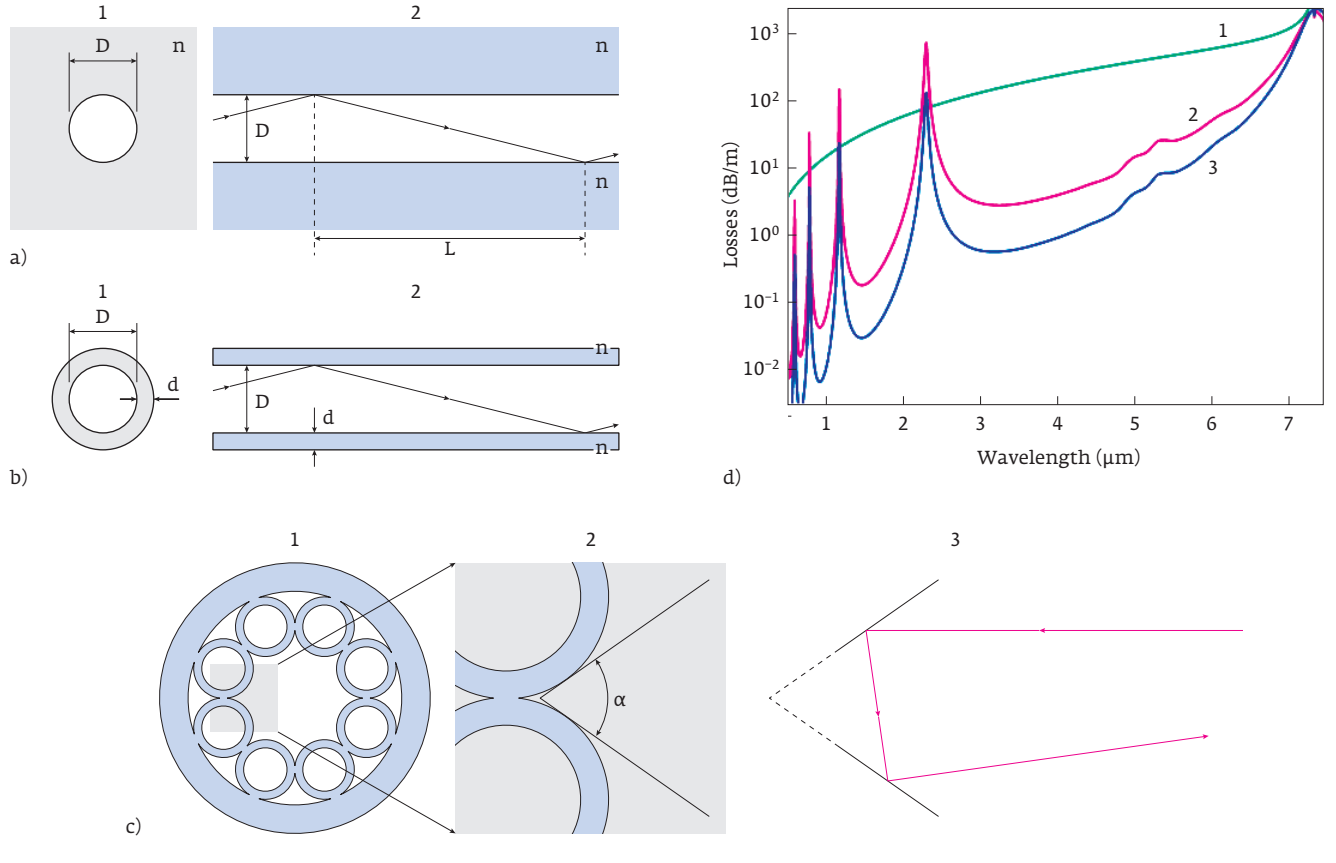

Fig. 2. *(a) Transverse (1) and longitudinal (2) sections of a hollow waveguide [10]; (b) - transverse (1) and longitudinal (2) sections of a tubular waveguide [12]; (c) transverse section (1) of the RF [1], approximation of part of the walls of the reflecting capillaries by the mirror sides of the angle a (2), reflection pattern of a beam propagating along the RF from the angle with the mirror sides-projection onto the cross section of the optical fiber (3); (d) - Calculated optical loss spectrum for silica glass waveguides: 1 - hollow waveguide (HWG), 2 - tubular waveguide (TWG) and 3 - revolver fiber (RF). For all waveguides, the diameter of the hollow core is assumed to be 77 μm, and the wall thickness of the capillaries (for TWG and RF) is 1.15 μm*

laries [7.8] (see Fig. 1 (c)). Finally, giving a thin glass wall at the core-cladding interface negative curvature when forming a reflective cladding from a capillary layer (PC [1]) preserves the band structure of the transmission spectrum, but leads to a further increase in the reflection coefficient at the core-cladding interface and, as a result, to further reduce optical fiber loss. Qualitatively, this can be explained as follows. The parts of the capillary walls located closer to the center of the core act as parts of the cladding in the TWG model. Parts of the walls of the capillary that deviate significantly from the circle inscribed in the core of the RF interact with electromagnetic radiation as sides of the angle with a highly reflective coating (see Figure 2 (c), 2). In the ray approximation, it can be said that light rays are reflected from these angular structures (see Fig. 2 (c), 3), and a decrease in the glide angle of the rays during reflection compared with reflection from portions of capillaries close to the center of the fiber leads to a significant lower optical loss compared to the TWG model.

Furthermore, when the capillaries in the cladding are separated by a distance $d<<(2\cdot\pi)/k_{\perp}$, where $k_{\perp}$ is the component of the wave vector perpendicular to the fiber axis, the conditions for the propagation of radiation along the core are practically unchanged compared to the cladding with contacting capillaries. This approximately corresponds to the removal of the vertex of the 'mirror' angle indicated by the dashed line in Fig. 2 (c), 3. However, in this case, the excitation of the cladding modes associated with the areas of contact of the capillaries with each other will be significantly reduced. All this results in a further effective reduction of optical losses in the RF. In an experiment, this result was first obtained in [4].

High coefficient about Friction at the core-cladding interface already in the case of HWG leads to the fact that the modes in the HWG are similar to the modes in ideally conducting metal fibers, when the radiation wavelength is far from the cutoff wavelength. This feature was noted in [10]. The RF, like any other fibers with negative curvature of the cladding, are characterized by an even greater reflection coefficient from the core-cladding interface. For this reason, the radiation power in the RF is even more concentrated in the hollow core. The optical absorption of the material from which the RF is made is fading into the background in these circumstances, while the losses in the RF are mainly caused by the emission of radiation from the core and are determined mainly by the geometrical parameters of the cladding and the conditions of its Fresnel reflection. This means that RF can be used to transport radiation and observe various optical phenomena even in those spectral regions where the material of the fiber (e. g., silica glass) is opaque.

As shown by the simplified RF models discussed above, the possibility of transmitting low-loss laser radiation in RF in the ultraviolet and mid-IR spectral ranges is mainly due to the value (taking into account changes in the spectrum) as real $\mathrm{Re}(n(\lambda))$ and imaginary $\mathrm{Im}(n(\lambda))$ parts of the refractive index of the fiber material. Note that the choice of material for RF is significantly limited: until now, RF has been made from quartz, chalcogenide [15] and organic glasses (polymethyl methacrylate) [16]. The waveguide properties are also affected by the ratio of the wavelength to the main geometric dimensions of the RF, such as the diameter of the hollow core D_{core} and the wall thickness of the capillaries d. However, this ratio can be optimized for the concerned wavelength in the process of creating the fiber.

For RF made of silica glass, optical losses in the mid-IR range increase with a wavelength of up to 7.3 μm (see Figure 2d). This occurs for two reasons: $\mathrm{Re}(n_{SiO_2})$ decreases [17], which leads to a decrease in the Fresnel reflection coefficient from the air-glass interface (here, the Fresnel reflection coefficient is mainly determined by the value of $\mathrm{Re}(n_{SiO_2})$, since the value of $\mathrm{Im}(n_{SiO_2})$ is small in compared to unit). Furthermore, the absorption of radiation in the wall of the quartz capillary begins to manifest itself in the wavelength region of about 5 μm. As a result, the efficiency of the ARROW mechanism decreases, and the value of the reflection coefficient from the capillary wall begins to decrease, approaching the values characteristic of the HWG model. This is also true for large wavelengths in the mid-IR range, with the exception of small areas of about 7.3 μm and possibly about 9 μm and 20 μm. Note that at these wavelengths, the value of $\mathrm{Re}(n_{SiO_2})$ is close to unity, and there is practically no reflection at the air-glass interface, so that hollow microstructured fibers (MSF) made of silica glass cannot exhibit any waveguide properties at these wavelengths.

In the near infrared and in the visible range, quartz glass fibers, like the quartz glass itself, work best. When dislocated along the wavelengths toward the UV range, the value of $\mathrm{Re}(n_{SiO_2})$ increases, which reduces the optical loss in the RF. However, at a wavelength of about 150 nm, the value of $\mathrm{Im}(n_{SiO_2})$ increases sharply, which, as in the mid-IR range, leads to the 'shutdown' of the ARROW interference mechanism. As a result, the value of optical losses increases to a level that is determined by only one reflection at the core-cladding interface (hollow fiber). Nevertheless, the results obtained show that quartz glass RF can be used up to vacuum ultraviolet (124 nm) [18]. In

the case of RF made of chalcogenide glass, the waveguide properties of RF were demonstrated up to wavelengths of ~10 μm [15]. Terahertz radiation can also be transmitted through waveguides made of polymers (e.g., polymethyl methacrylate), structurally similar to RF [16].

3. RF WITH VARIOUS DESIGNS OF REFLECTIVE CLADDING

The spectral properties of RF were studied in detail by numerical modeling and experimentally. Optical loss is one of the main parameters of RF. Fig. 3 shows the experimentally achieved optical losses to date in HCF of various types of silica glass, including RF. For comparison, the absorption spectrum of pure silica glass is also shown. As seen in Fig. 3, in the ultraviolet range, the optical losses of RF (Fig. 3, data 15) approach the absorption level of pure quartz glass (Fig. 3, data 2). Note that HCF having a square (data 14) and hexagonal (data 11) core without negative curvature demonstrate properties similar to those of the RF here. In the near infrared range, optical fibers with photonic band gaps (PCF) (data 6) have the lowest optical loss. At wavelengths of 3–4.4 μm in the mid-IR, both RF (data 5, 16, 17) and HCF with elements of the cladding structure in the form of an "ice-cream cone" (data 8) show the same optical losses, which are lower than in pure quartz glass (data 3). It is worth noting that RF (Fig. 3, data 4, 16) are the only hollow quartz fibers that exhibit optical transmission at wavelengths above ~4.4 μm.

Fig. 3 shows that RF expand the applicability of quartz fiber optical fibers to the mid-IR range (above ~3 μm). For example, at a wavelength of 4.4 μm, where the absorption coefficient of silica glass is about 4000 dB/m (Fig. 3, data 3), RF made of silica glass allowed for demonstration of optical losses at the level of 1 dB/m (Fig. 3, data 16). It should be noted that in comparison with RF made of quartz glass, solid-state optical fibers from special types of glasses can have lower optical losses in the mid-IR range. For example, optical losses of less than 0.1 dB/m have been demonstrated in fluoride fibers in the spectral range of 2.0–4.5 μm [36] with wavelengths up to 6.5 μm in chalcogenide fibers [37, 38]. In the longer wavelength range (8–16 μm), silver halide optical fibers exhibit optical losses below 1 dB/m [39]. As a rule, all-glass non-quartz optical fibers intended for mid-IR range can provide 10–1000 times lower losses than those in the RF made of quartz glass. However, the use of silica glass RF can be beneficial at wavelengths of up to ~5 μm, since a reasonable level of optical attenuation can be achieved using well-developed technology. Moreover, the damage threshold in RF is much higher in comparison with all-glass non-quartz optical fibers for mid-IR range. Thus, hollow RF are indispensable for applications related to the transportation of high-power radiation.

3.1. RF with contacting and non-contacting capillaries in the cladding

After the first RF that had contiguous capillaries in the cladding (Fig. 1 (a)) [1], a modified RF with non-contacting capillaries in the cladding (Fig. 1 (b)) was proposed [4]. It turned out that this kind of the RF structure has lower optical losses than the previous one. Subsequently, RF with non-contacting capillaries in the cladding were used in many researches (see, e.g., [32, 34, 40]).

By numerical modeling it was shown that the absence of common points between the capillaries eliminates additional resonances in the passbands (Fig. 4). In the course of numerical modeling, two models of RF were compared. There, all the geometric parameters of the RF were identical, except that the gaps between the capillaries in one of the optical fibers (red line in Figure 4) were filled with glass (see the detail in Figure 4). Thus, the whole difference between the two curves in Figure 4 (a) is determined by the presence of nodes between the capillaries in the

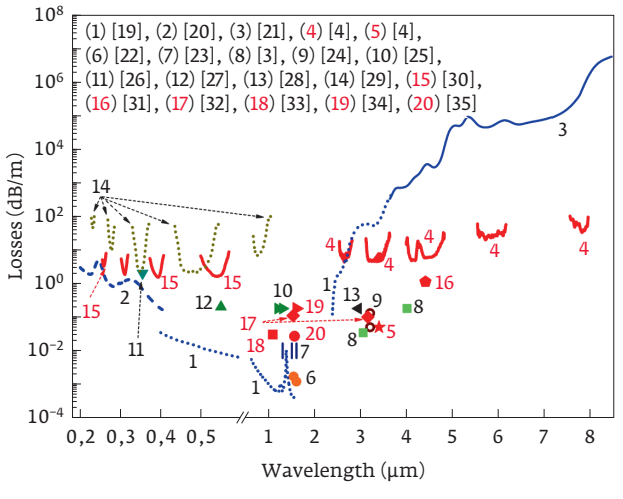

Fig. 3. *Optical losses in pure quartz glass (F300, Heraeus, Hanau, Germany) (blue curves, 1–3) and the minimum optical losses obtained to date in various types of hollow silica glass fibers (HCF). RF data is highlighted in red. In the legend of the figure, the experimental data are indexed by numbers in parentheses, followed by references to the literature in square brackets. See the text for more information*

cladding. The cladding of each fiber consisted of eight capillaries, which had outer and inner diameters of 63 μm and 51 μm, respectively. The minimum distance between non-contacting capillaries was 1.3 μm. The loss spectra were calculated in the spectral range of 3–6.5 μm for both RF. The modeling results show that the presence of nodes between the capillaries leads to an increase in the optical loss of the fiber due to resonances between the core and cladding modes.

For the first time, RF with individual capillaries in the cladding was fabricated in [4]. The fiber had an outer diameter of 290 μm, a core diameter of 110 μm, and a capillary wall thickness of 6 μm. The fiber cross-section and the measured spectrum of optical losses are shown in Fig. 5. It can be seen that the average level of optical losses measured in the spectral range of 2.5–5 μm was about 4–5 dB/m. In the longer wavelength range of about 5.8 and 7.7 μm, the measured losses were 30 and 50 dB/m, respectively. The passband at 3.3 and 4.3 μm has a number of absorption peaks that are associated with the absorption lines of HCl (similar to [3]) and atmospheric CO_2, respectively. The optical absorption of silica glass is also given for comparison (Fig. 5, black curve).

To analyze the experimental results, a numerical simulation of optical losses was performed for the fundamental mode of this fiber (Fig. 5, green curve). As can be seen from Fig. 5, the calculated and experimentally obtained edges of the passband coincide well. On the other hand, data on the minimum level of loss in bandwidths are significantly different. Apparently, this is mainly due to the presence of higher-order modes during loss measurement (during the experiment, a multimode light source was used to excite a short section of the fiber). This explanation is consistent with the results of loss measurements by the cut-back method using a low-mode He-Ne laser (3.39 μm) in an 11-meter fiber. This experiment showed that at the indicated wavelength, the composition of the modes in the fiber is stabilized at the fiber length over 3 m. When only the first few modes are present in the fiber, the loss level is only 50 dB/km (red star in Figure 5), which is much closer to the loss level estimated for the main mode at 3.39 μm. Thus, the level of real losses in the fiber with a low-mode mode of propagation of light is quite low and can be estimated using the estimated loss spectrum (Fig. 5, green curves).

3.2. RF with single and double embedded capillaries

In the mid-IR spectral range, the material losses of silica glass vary from 0.1 dB/m to 105 dB/m for wavelengths from 2 μm to 6 μm [41]. Thus, the total losses in silica glass RF, starting from wavelengths >2 μm, are increasingly determined by the material losses of silica glass. In this case, the designs of ordinary revolver optical fibers ((Fig. 1 (a) and (b)) and optical fibers with embedded capillaries in the cladding (Fig. 1 (c)) behave differently in the region of high material losses of silica glass [41]. RF with embedded capillaries transmit radiation with losses smaller than in a conventional RF, up to a certain wavelength in the mid-IR range. In this case, the second capillary acts as a second reflecting surface and an increase in the reflection coefficient from the cladding gives a gain in total losses over the average with ordinary RF (with single capillaries, Fig. 1 (a, b)). With a further increase in the wavelength and, therefore, the level of material losses, the second reflecting wall of the embedded capillary of the RF can no longer compensate for the growth of material (and total losses, respectively). That is why the first hydrogen Raman laser with a generation wavelength of 4.4 μm [31, 42, 43] was built on the basis of an ordinary RF with one layer of capillaries. It was shown in [4] that revolver silica glass fibers allow transmission of radiation up to a wavelength of 8 μm with losses of the order of several tens of dB/m (Fig. 5). For practical applications of silica glass RF in this spectral region, this loss level is too high. Therefore, it is believed that for the RF made of silica glass, the applicability limit is limited to a wavelength of approximately 5 μm, since in the region of this wavelength, the material losses of silica glass increase by approximately an order of magnitude compared to

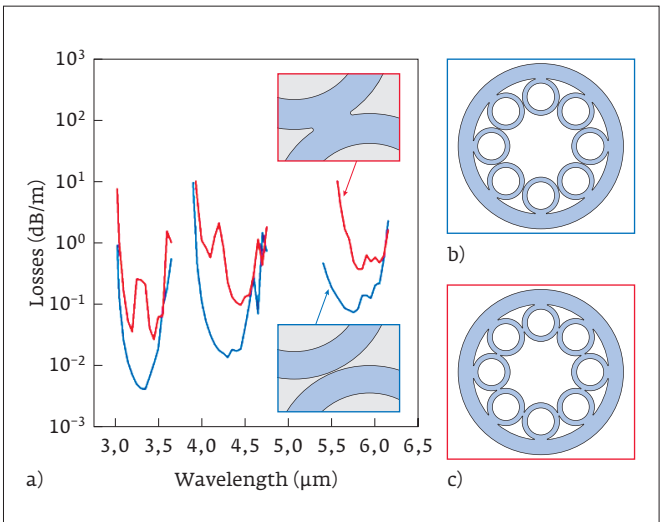

Fig. 4. (a) Estimated losses of the main modes for quartz RF with adjacent and non-contacting capillaries in the cladding; (b) and (c) are cross-sections of these RFs

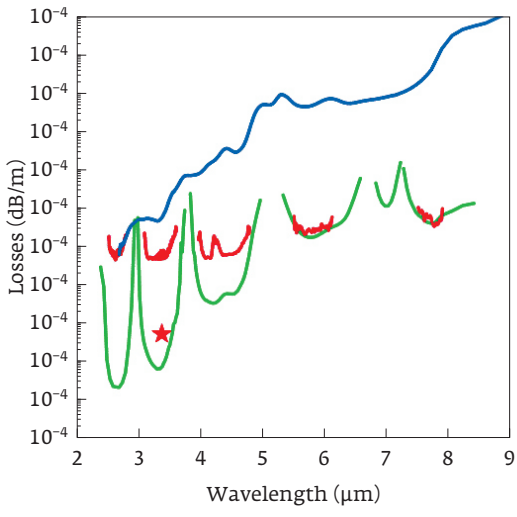

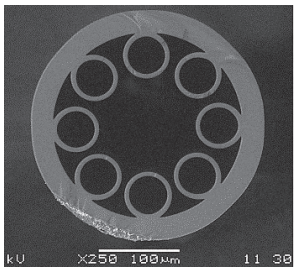

Fig. 5. *(a) measured losses (red); losses measured with a 3.39 μm He-Ne laser (red star); material losses in quartz glass (black); estimated losses of the main RF mode (green); (b) photograph of the RF cross-section, D_{core} = 110 μm, the wall thickness of the capillaries d = 6 μm*

previous values (Fig. 5 (a)). Thus, in the transparency region of quartz glass, RF with double embedded capillaries exhibit lower optical losses compared to RF with single ones. In the field of high optical losses in quartz glass, RF with single capillaries have an advantage. In addition to the above, the influence of bending losses must always be taken into account.

In order to pass radiation through a quartz glass revolver fiber in the mid-IR range, in the region of a wavelength of 5 μm, with acceptable losses at the level of ~1 dB/m, it is necessary to optimize the geometric structure of the cladding: the capillary wall thicknesses giving the desired transmission zone at given wavelength, the distance between the capillaries, their number and size of the hollow core. Another way to solve the problem of transmitting radiation in revolver optical fibers in the mid-IR range with low losses is to use special glasses (chalcogenide, tellurite), which have small material losses in this range.

3.3. RF properties in the UV wavelength range

A somewhat different situation is observed when radiation is transmitted in the UV spectral range. The measured material losses of silica glass in the spectral range from 200 to 400 nm are not as large as in the mid-IR spectral range and vary in the range from a few tenths to ~10 dB/m [20]. Therefore, comparing the role of waveguide and material losses, it can be stated that waveguide losses play a major role in this case. Thus, the main mechanism to reduce the level of total losses in this case is the optimization of geometric oh structure of quartz glass RF. On the one hand, low waveguide losses can be obtained by increasing the diameter of the hollow core, which is much larger than the considered wavelength. On the other hand, this leads to the excitation of a large number of modes of the hollow core due to the heterogeneity of the fiber structure arising during its drawing, as well as to the narrowing of the transmission zones of the fiber [30]. Therefore, as in the case of RF in the mid-IR range, it is necessary to choose some optimal design with a certain wall thickness of the capillary wall to comply with all the above conditions, with certain distances between the capillaries and with a certain diameter of the hollow core. The use of RF with embedded capillaries in this spectral range seems unlikely due to the complexity of their manufacture (e.g., maintaining the size and shape of the cladding capillary during drawing). Furthermore, the number of capillaries in the cladding is also important. For example, in [44], the waveguide mode in quartz glass RF was demonstrated with four capillaries in the cladding with losses of about 0.5 dB/m at a wavelength of 350 nm. But the size of the capillaries compared with the diameter of the core is such that the loss in bending should be large. In RF, demonstrated in [30], with a hollow core diameter of 15 μm and eight capillaries in the cladding, several transmission zones were observed in the UV range from 200 to 350 nm. Losses were at the level of 1–2 dB/m. The authors attribute such a rather high level of waveguide losses to the imperfect design of the drawn fiber. In conclusion, it is worth to mention the polygonal fiber, localizing light due to the so-called double antiresonant mechanism [29]. The authors of [29] proposed the use of a fiber with a square core-cladding boundary suspended on special

struts attached to a support tube. This fiber gave a system of transmission zones up to a wavelength of 241 nm, with losses comparable to those in the RF presented in [30].

4. DESIGN AND FABRICATION OF RF

To date, most fiber optic revolver fibers have been made of quartz glass. Significantly greater difficulties arise in the manufacture of RF from glasses of other types, e.g., chalcogenide. The processes of fabrication of these fibers are considered further.

4.1. Quartz glass RF fabrication technology

One of the significant advantages of RF over, e.g., Kagome-type optical fibers is the simpler structure of the optical fiber and, therefore, a simpler technology for their fabrication, since the reflective cladding contains only one layer of capillaries.

Workpieces for RF are made by assembling from capillaries. To this end, prefabricated capillaries are inserted into the support pipe (see Fig. 6). In this case, the capillaries can either abut against each other (Fig. 6a), or at the beginning and at the end of the assembly additional auxiliary bursting elements can be inserted between the capillaries (Fig. 6b). In the first case, a fiber with contacting capillaries [1] or an ice-cream cone structure [3] is obtained, in the second case, a revolver fiber with spaced capillaries [4] is possible. Furthermore, both simple single capillaries (Fig. 6a) and capillaries of a more complex design, e.g., double embedded capillaries (Fig. 6b), can be used to fabricate a fiber. The result is either single-capillary RF that work better in the areas where the intrinsic absorption of silica glass is of great importance, or double-capillary RF that provide less optical loss in the spectral regions where absorption in quartz glass is not yet decisive for losses in the RF.

After the assembly stage, the workpiece undergoes primary heat treatment in order to weld the capillaries to the carrier tube, however, this procedure is optional, e.g., in [15], when fabrication RF from chalcogenide glass, the capillaries were not welded because of the fear of cracking of the workpiece after such heat treatment.

In the process of drawing a fiber, excessive gas pressure is supplied inside capillaries to prevent them from collapsing under the action of surface tension forces. Usually, this is done via a gas pressure regulator, which is connected to all capillaries and maintains the necessary overpressure. This approach has a significant drawback that does not allow fabricating RF with exactly the same capillaries. Obviously, the capillaries used for the fabrication of the workpiece inevitably have size deviations from the average value, therefore, the surface tension forces tending to collapse the capillary will differ for each capillary, which means that for each capillary it is necessary to use an individual pressure control system, which is difficult to practically implement. As a rule, in practice, the same pressure is applied to all capillaries, and the scatter of capillary sizes in the workpiece increases during the drawing of the fiber (see Fig. 7, upper arrow). This is because capillaries having a diameter less than the average decrease their relative size even more during the drawing process, and capillaries with a size higher than the average increase during the drawing process (the average means the diameter of the capillary at which the surface tension forces are balanced by internal overpressure). Nevertheless, the use of high-quality tubes (e.g., Heraeus quartz pipes) as a 'feedstock' for the manufacture of capillaries allows one to achieve good results even by technology with the same pressure being applied to all capillaries.

There is an alternative approach to the extraction of microstructured optical fibers, which is also applicable to the RF drawing. The method is called the 'technology of drawing with top end sealed' (Fig. 7, lower arrow) [45]. The essence of this technology is that the cavity of the workpiece is sealed from the top end of the workpiece. Thus, each cavity initially contains a certain amount of gas and all cavities are isolated from each other. During the drawing process, the lower part of the workpiece is heated, the pressure in the cavities increases, and the cavities themselves expand. The degree of increase in the volume of the cavity is determined by the ratio of the temperature of the top end of the workpiece to the temperature in the waist zone (in the bulb) and, to a first approximation, does not depend on the diameter of the cavity. In other words, all the workpiece cavities at each instant of time increase by the same number of times [45]. Thus, the scatter in the size of the capillaries available in the RF workpiece is also preserved in the fiber. Whereas when using technology with the same pressure applied to all capillaries, the deviation of the capillary sizes from the average value increases with the drawing of the fiber.

A significant drawback of the 'technology of drawing with top end sealed' is that during the drawing process the top, initially cold end of the workpiece approaches the hot zone and heats up, and as a result, the degree of inflation of the cavities decreases. That is, the RF drawn using this technology have a smoothly varying capillary size along the length of the fiber.

4.2. Fabrication technology and RF properties based on chalcogenide glasses

Although the waveguide mode of propagation in a revolver fiber made of quartz glass up to a wavelength of 7.9 μm was demonstrated in [4], the optical loss in the revolver fiber is more than 10 dB/m at wavelengths greater than 4.5 μm. Apparently, it is impossible to construct a hollow fiber waveguide from quartz glass with reasonable dimensions, which would have an optical loss of ~1 dB/m at wavelengths greater than ~5 μm. Therefore, to move further into the longer wavelength range of the spectrum, it is necessary to develop hollow fibers from other materials. Tellurite glasses have a wider transparency region [46]. Their use allows for advancing to a wavelength of 5.5–6 μm. But a more radical gain comes from the use of oxygen-free glasses, chalcogenide ones in particular.

The situation with technology is becoming much more complicated. Both the quality of the initial chalcogenide glass tubes and their physical properties lead to the fact that obtaining RF from them with geometric parameters comparable in quality rather than in accuracy with the parameters of RF from quartz glass is a much more difficult task (which can be seen by comparing the cross-sections of the quartz fibers in Figures 6 (c) and (d) and chalcogenide in Figures 8 (b) and (d)). The first chalcogenide glass revolver fiber was manufactured in 2011 [15]. High-purity glass $As_{30}Se_{50}Te_{20}$ was used for its fabrication, the fiber was made using "stack and draw" method. The support tube was made by centrifugal casting inside an evacuated quartz tube. The capillaries were made by the double crucible method from a chalcogenide glass melt. The elimination of the stage of obtaining a glass tube by centrifugation for the drawing of capillaries has reduced the likelihood of crystallization of chalcogenide glass and, thereby, the total optical loss in the fiber. The pre-form was an assembly of a supporting glass tube and 8 capillaries with a given geometry and wall thickness located in one layer near the inner wall of the supporting tube (Fig. 8 (a)).

An optical fiber with an outer diameter of 750 μm and a core diameter of 260 μm was drawn from the pre-form assembly obtained, the capillary wall thickness was 13 μm (see Fig. 8 (b)). The optical loss in this fiber was 11 dB/m at a wavelength of 10.6 μm. The optical fiber carried the CO_2 laser radiation through the hollow core, which was recorded using a thermal imager Fig. 8 (c).

Then, in 2014, using a similar technique, a fiber was manufactured from a simpler and more technologically advanced chalcogenide glass As_2S_3 [47] (Fig.

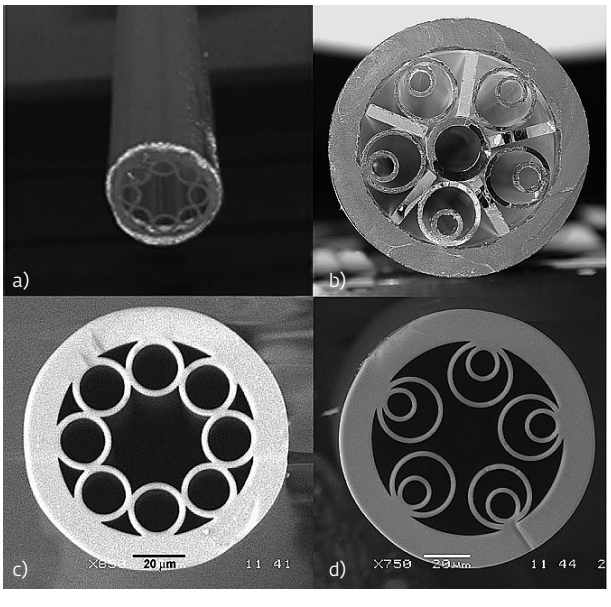

Fig. 6. *Cross-sections of optical elements at the main stages of fabricating RF with double embedded and single capillaries. (a) photograph of a RF workpiece with single capillaries adjacent to each other; (b) photograph of the assembled RF workpiece with quartz elements between double capillaries, Ø25 mm; (c) an image of a cross-section of a drawn RF obtained with a scanning electron microscope (SEM) with contacting capillaries (from the workpiece shown in Fig. 6 (a)); (d) an image of a section of a drawn RF with double embedded non-contacting capillaries obtained with a scanning electron microscope, Ø110 μm (from the workpiece shown in Fig. 6 (b))*

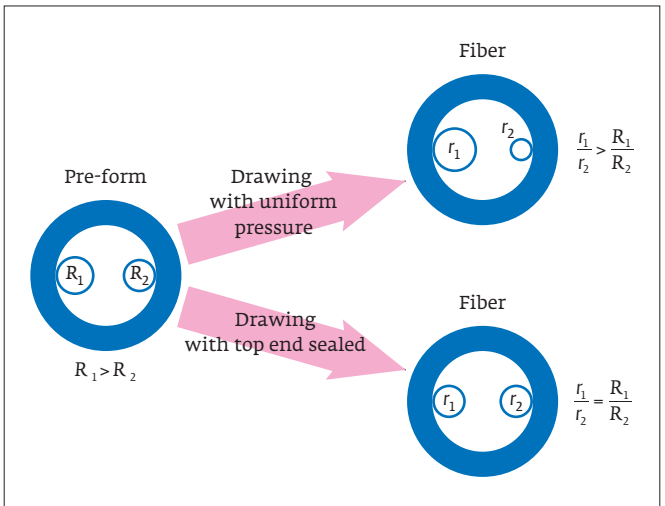

Fig. 7. *Illustration of RF drawing with the uniform pressure applied to all capillaries (above) and RF drawing with top end sealed (bottom)*

8 (d)). The minimum optical loss in this fiber was 3 dB/m at a wavelength of 4.8 μm, and absorption bands of typical impurities are observed in the fiber loss spectrum, e.g.: S-H bands at 6.8; 4.1; 3.7; 3.1 μm; bands from CO_2 admixture at 4.31 and 4.34 μm; OH groups at 2.92 μm; COS at 4.9 μm, molecular H_2O at 6.33 μm. This suggests that a significant proportion of the power in this fiber is spread over the glass.

In 2015, Gattass et al. used extrusion technology to produce the pre-form of a revolver fiber from As_2S_3 glass [48]. As a result, a pre-form with a diameter of 18 mm and a length of 135 mm was obtained (Fig. 9 (a)). The fiber drawn from this pre-form had the following geometric dimensions: the core diameter was 172 μm, the sizes of oval capillaries were 70 by 75 μm, and the capillary wall thickness was 7 μm (Fig. 9 (b)). Optical losses were 2.1 dB/m at a wavelength of 10 μm.

In all researches with chalcogenide RF, theoretical calculations of optical losses were carried out using the finite element method. In this case, the experimentally measured losses are almost always several orders of magnitude higher than the theoretically calculated values. The observed difference is explained by the strong sensitivity of the optical properties of the fiber to variations in the geometric parameters of the resulting structures. The increased sensitivity of chalcogenide fibers to variations in geometric parameters compared to quartz fibers is due to the high refractive index of chalcogenide glasses, i.e. with the same absolute variations in geometric thicknesses, variations in optical thicknesses in chalcogenide fibers are by 3–4 times greater than in quartz fibers. Furthermore, the temperature dependence of the viscosity of chalcogenide glasses is several times sharper than the temperature dependence of the silica glass viscosity (chalcogenide glasses are 'short'), i.e. at the same temperature gradients and temperature fluctuations during the drawing process, the quality of chalcogenide microstructured fibers is lower than that of quartz. It is also obvious that the purity and uniformity of the chalcogenide glasses used is significantly inferior to the purity and uniformity of high-quality quartz glass used in the manufacture of RF.

In all works on chalcogenide RF, the loss spectra obtained as a result of theoretical modeling contain frequent resonant peaks. This fact is explained by the resonant coupling of the hollow core modes with cladding modes. Similar resonance peaks are sometimes observed in theoretically calculated loss spectra of quartz revolver optical fibers at the long-wavelength edge of transmission bands [9] (see also [4], Fig. 4). However, in the case of chalcogenide fibers, the cut-off of transmission spectra is almost always observed in mathematical modeling. This is because the set of cladding modes in the case of chalcogenide RF is denser due to the high refractive index of chalcogenide glasses. But in the experiment, narrow peaks of optical loss in the transparency zones of chalcogenide RF were never observed. Apparently, due to the poor geometry of the fabricated fibers, the real peaks in the loss spectra are broadened.

5. RF-BASED RAMAN FIBER LASERS OPERATING IN THE MID-IR RANGE

When comparing the optical losses in pure quartz glass and hollow core optical fibers (see Fig. 3), we can see that if in the UV range the achieved losses for HCF are only comparable to the losses in v-SiO_2, then in the mid-IR range HCF have several orders of magnitude lower losses and, in fact, open up possibilities for silica glass fibers for operating in the mid-IR range, in particular for the creation of lasers. Moreover, at present, most of the smallest values of experimentally obtained data on HCF losses in the mid-IR range belong to RF (Fig. 3).

Gas fiber lasers can be designed based on HCF. Such lasers are capable of combining the advantages of both fiber lasers (compactness, reliability, single-mode radiation) and gas lasers (a wide range of generation wavelengths, high output power, and a small

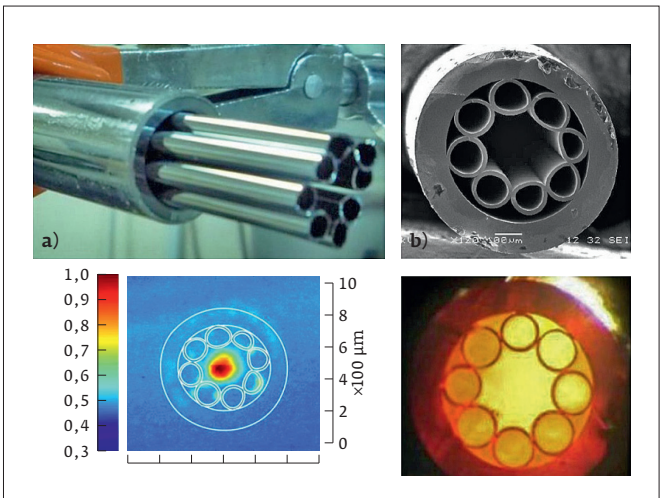

Fig. 8. a) RF workpiece of glass $As_{30}Se_{50}Te_{20}$, outer/inner diameter of the pipe 16/11 mm, outer/inner diameter of the capillaries 3/2.4 mm; b) a photograph of the RF obtained from this workpiece. The outer diameter of the fiber is 750 μm; c) intensity distribution of the CO_2-laser radiation at the output of a given fiber (in the production unit). On top of the distribution there is a schematic representation of the given RF; d) photograph of a cross-section of an As_2S_3 glass fiber. The outer diameter is 820 μm

generation line width). The active medium of gas fiber lasers is gas that fills the hollow core of the fiber and has dipole-active or Raman-active transitions. In this case, the hollow fiber provides a small diameter of the mode field and a long interaction length of radiation with the active medium, as a result of which the thresholds for the generation of lasers at active centers and the thresholds of nonlinear processes, such as, for example, stimulated Raman scattering (SRS), can be reduced by several orders of magnitude compared to non-waveguide schemes.

Currently, active research is underway to create mid-IR gas fiber lasers based on the Raman effect in gas-filled HCFs. In particular, the RF-based Raman lasers are shown that generate at wavelengths from 2.9 to 4.4 μm [42, 43, 49].

In most works, gas fiber lasers are created according to a non-resonator single-pass scheme [5, 50–53]. Due to the high localization of radiation in the core (d~5÷50 μm) throughout the entire length of the fiber (~1–10 m), hollow fibers filled with active gas provide amplification in one pass, sufficient for the development of generation from quantum noise. Thus, the single-pass scheme allows one to implement efficient gas fiber lasers (GFL) based on both SRS [5, 50, 52] and population inversion [51]. Currently, the creation of a resonator for GFL remains a technically challenging task, since there are no components such as fiber couplers and analogues of fiber Bragg gratings for hollow fibers. Nevertheless, in several researches, resonator patterns of GFL using a ring resonator on bulk elements [40] and a resonator formed by Bragg gratings welded to the ends of the active hollow fiber [54] were studied.

As the active medium of gas fiber Raman lasers, light molecular gases such as light hydrogen ($^1H_2$), deuterium (D_2), methane (CH_4) or ethane (C_2H_6) are of interest, since they have a large Raman shift (4155 cm^{-1}, 2987 cm^{-1}, 2917 cm^{-1} and 2954 cm^{-1}, respectively). This circumstance opens up the possibility of creating single-stage mid-IR Raman lasers, the pump source for which can be pulsed nanosecond erbium fiber lasers that generate about ~1.5 μm in a well-developed spectral range.

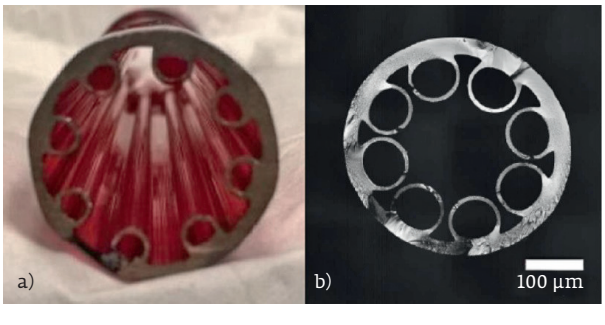

Fig. 9. *(a) An optical fiber pre-form obtained by extruding from As_2S_3 glass; (b) RF made of As_2S_3 glass [48]*

A key component for creating efficient mid-IR Raman lasers is a hollow fiber, the characteristics of which must satisfy certain conditions. A necessary condition for SRS generation is the excess of SRS gain over the amount of optical loss in the fiber. It is known [55] that a kind of quality parameter (P_F)) can be introduced that characterizes a fiber as a medium with SRS amplification:

$$P_F = \left(\sqrt{\frac{\alpha(\lambda_p)}{g_0}} + \sqrt{\frac{\alpha(\lambda_s)}{g_0}} \right).$$

P_F is expressed in terms of the fiber parameters: optical losses at the pump wavelength $\alpha(\lambda_p)$, at the Stokes generation wavelength $\alpha(\lambda_s)$ and the Raman gain of the fiber g_0 (e.g., in dB/(m×W)) for the Raman conversion $\lambda_p \rightarrow \lambda_s$. The physical meaning of the value of P_F having a power dimension (W) is as follows: this is the threshold pump power for a Raman laser on the considered optical fiber placed in some high-Q resonator. Therefore, the smaller the value of P_F, the closer the fiber in its characteristics to the optimal for the selected Raman transform $\lambda_p \rightarrow \lambda_s$.

It is known that for direct (i.e., not bent) HWG and TWG optical losses depend on the diameter of the hollow core as $1/D^3$ and $1/D^4$, respectively [12, 14, 56]. Therefore, for both the HWG and TWG models, in the case of direct fiber, the quality parameter P_F is proportional to $1/D$ (for HWG) and $1/D^2$ (for TWG), because g_0 is proportional to $1/D^2$ (if the effective fiber area is proportional to D^2). Therefore, the more D is, the less is P_F. Thus, there is no optimum for direct optical fibers depending on the diameter of the hollow core. The situation changes if we take into account the losses caused by the bending of the fiber. The ability to bend is one of the main advantages of optical fibers. Assuming that we are working with HWG and TWG that are wound with a certain radius R, the bending losses in such fibers are proportional to the diameter of the hollow core D. As a result, the optical losses of such fibers have a minimum at some value of the diameter of the hollow core at any specific wavelength. Therefore, the quality indicator P_F reaches its minimum value at a certain diameter of the hollow core D_{min}, which determines the optimal diameter of the fiber core for the Raman conversion. If we take R=15 cm, and the

hollow core is filled with hydrogen at a pressure of 30 atm, then using the HWG and TWG models, we will obtain D_{min}>>75 for both models. A much more complicated numerical modeling of real RF gives approximately the same value [57].

It is important that the value of P_F should be significantly lower than the available pump radiation power. Let us estimate the parameter P_F for a model fiber with a hollow core diameter of ~75 μm (Ae_{ff}~2.4 ·10^{-5} cm^2) filled with molecular hydrogen at room temperature and pressure ≥10 atm (g_R~1 cm/GW, $g_0=g_R/A_{eff}$). Considering the optical losses $\alpha_p \leq 0{,}1$ dB/m (near IR) and $\alpha_s \leq 1$ dB/m (mid-IR) in principle achievable in such a fiber, we obtain the quality parameter $P_F \leq 100$ W. Peak radiation power that is many times greater than this value can be achieved using existing solid-state and fiber nanosecond pulsed lasers. However, it should be noted that the creation of quartz hollow fibers with an optical loss level of ≤1 dB/m in the mid-IR range is a non-trivial task, since the material absorption of quartz glass in the wavelength range of 3–5 μm sharply increases from ~50 to ~50,000 dB/m. Nevertheless, RF with approximately similar parameters were created and served as the basis for the first mid-IR Raman lasers.

Up to now, single-pass patterns similar to those shown in Fig. 11 have been used in Raman mid-IR lasers [58]. In [49], [58], a quartz revolver fiber was used as an active fiber, the theoretical transmission spectrum of which is shown in Fig. 10 (a). The fiber length was 15 m; the diameter of the mode field was 45 μm. When the hollow core was filled with molecular deuterium D_2 (partial pressure of 28 atm) with an admixture of molecular light hydrogen $^1H_2$ (partial pressure of 2 atm), SRS generation was obtained at wavelengths of 2.9, 3.3, and 3.5 μm (Fig. 10 (b)). The peak power of the most intense spectral components in the mid-IR was 0.25 kW (λ=2,9 μm) and 0.37 kW (λ=3,5 μm), which corresponds to an average power of 23 and 37 mW, respectively. The quantum conversion efficiency was 10% (for λ=2,9 μm) and 6% (for λ=3,5 μm) and allows for further optimization. Note that by selecting the partial pressures of the gases $^1H_2$ and D_2 and adjusting the pump power, it was possible to achieve predominant generation at a wavelength of 2.9 or 3.5 μm.

In [42, 59, 60] the RF structure was modified in such a way as to shift its transparency region to the region of ~4 μm (Fig. 12a). The diameter of the fiber mode field was 56 μm. In the fiber, when it is filled with molecular hydrogen $^1H_2$ at a pressure of 30 atm in a pattern similar to that shown in Fig. 11, Raman generation was first obtained at a wavelength of 4.4 μm (Fig. 12b) [42.60]. Using single-mode radiation from this laser, the optical losses of RF were measured at a wavelength of 4.4 μm, which turned out to be 1.13 dB/m, in good agreement with the results of numerical modeling of such fiber (0.92 dB/m) [59]. The length of the used RF in these experiments was 15 m.

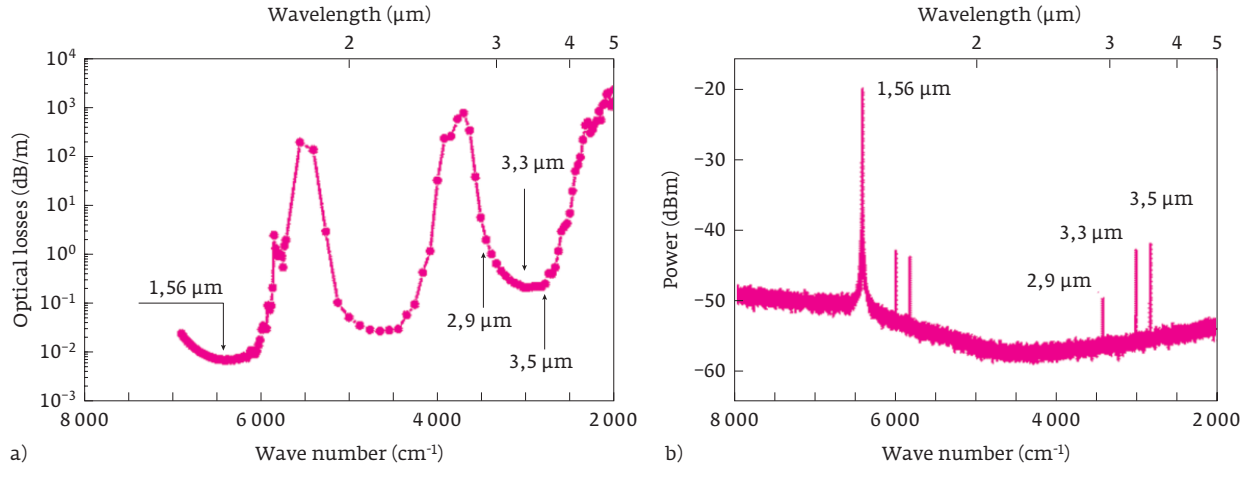

Fig. 10. *(a) The optical loss spectrum of a hollow core fiber, designed to create a GFL in the spectral region of 2.9 – 3.5 μm [49, 58]; (b) - The emission spectrum measured in [58] at the output of a gas fiber Raman laser. A mixture of molecular deuterium and light hydrogen at room temperature and partial pressures of 28 and 2 atm, respectively, was used as the active medium. The peak pump power at a wavelength of 1.56 μm was 14 kW*

By numerically solving the system of equations of coupled waves for vibrational Raman scattering in molecular hydrogen $^1H_2$, a theoretical analysis of the Raman scattering was made at a wavelength of 4.4 μm. In this case, the measured optical loss values of 0.04 dB/m and 1.13 dB/m at wavelengths of 1.56 and 4.4 μm, respectively, were used (Fig. 12), as well as the value of the Raman gain g_R=0,43 cm/GW, calculated for the conversion of 1.56 → 4.4 μm based on the known data on the line width and scattering cross-section for the vibrational transition Q(1) of the $^1H_2$ molecule [61–63]. The optimal Raman laser length obtained by theoretical analysis was about 3.5 m, which is significantly less than the length of the hollow fiber (15 m) used in the experiment [42, 43].

One of the interesting results of [59] is the ability to maintain a stationary SRS mode when pumping gas fiber lasers with nanosecond pulses. It is known [61] that if the duration of the pump pulse (τ_p) and the transverse relaxation time of optical phonons (T_2) satisfy the relation $\tau_p \leq 20 \cdot T_2$, then the SRS transition goes into a non-stationary mode, in which the coefficient of SRS gain is reduced. For the vibrational transition Q(1) in molecular hydrogen at room temperature and a pressure of ~10 atm, the transverse relaxation time is $T_2 \approx 0{,}64$ ns and, as a result, pump pulses of a few nanoseconds duration should lead to unsteady SRS generation. However, the time T_2 can be easily controlled by changing the gas pressure, since with increasing pressure, the collision frequency of molecules increases, which leads to a more frequent failure of the phase of molecular vibrations and, therefore, reduces the value of T_2. The indicated effect was observed in [59] with a change in the hydrogen pressure in the range 10–70 atm and made it possible to increase the output power

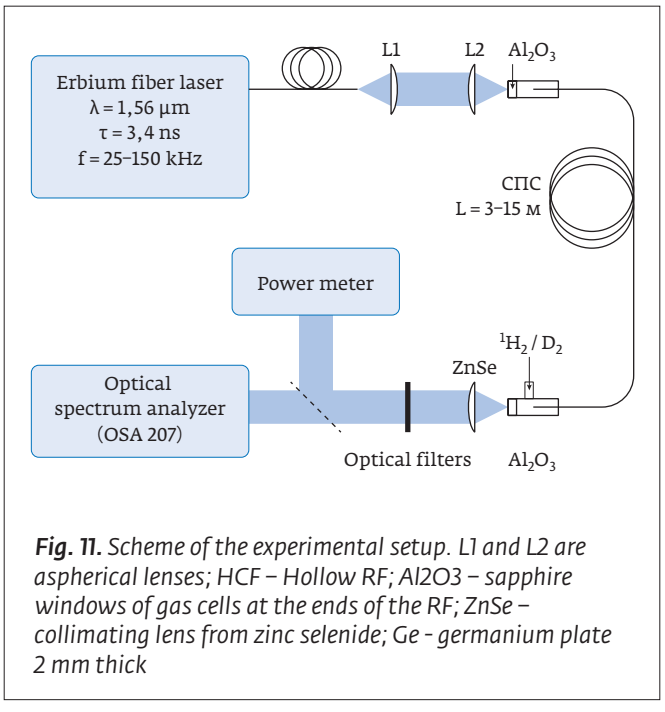

Fig. 11. *Scheme of the experimental setup. L1 and L2 are aspherical lenses; HCF – Hollow RF; Al2O3 – sapphire windows of gas cells at the ends of the RF; ZnSe – collimating lens from zinc selenide; Ge - germanium plate 2 mm thick*

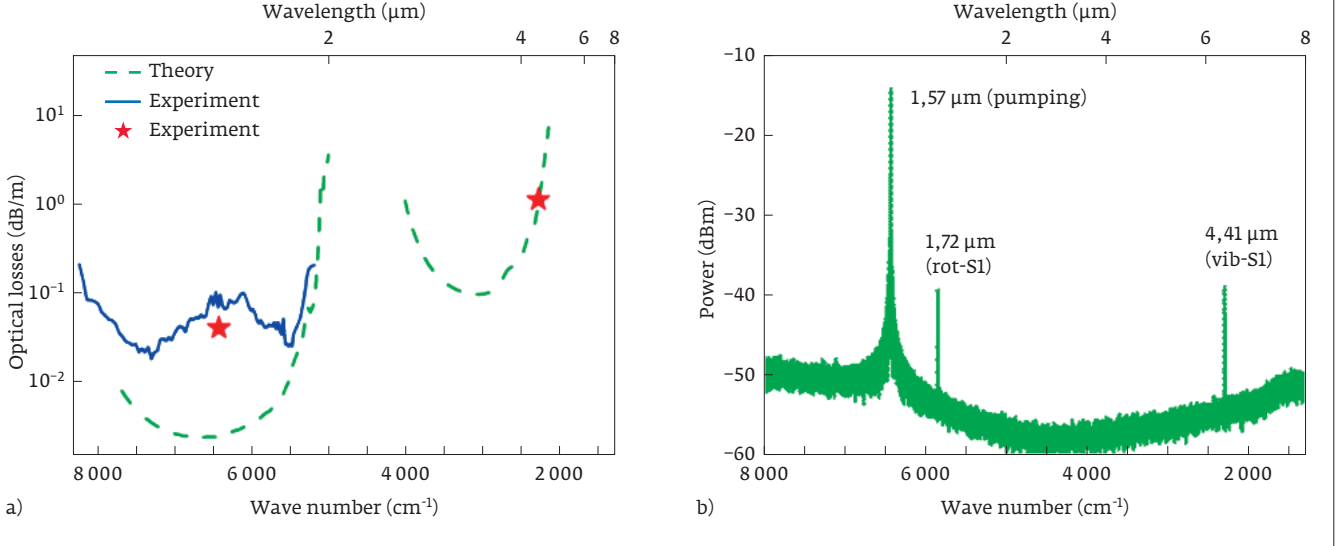

Fig. 12. *(a) Calculated optical loss spectrum of a hollow core revolver fiber (black dashed line) [43]. Also shown is the loss spectrum measured using a supercontinuum source in the near-IR range (blue line). The red star represents the optical losses measured using narrow-band laser sources at wavelengths of 1.56 and 4.4 μm [59]. (b) The emission spectrum at the output of a RF filled with $^1H_2$ light hydrogen at room temperature and a pressure of 30 atm. The introduced peak pump power was 18 kW [42, 43]*

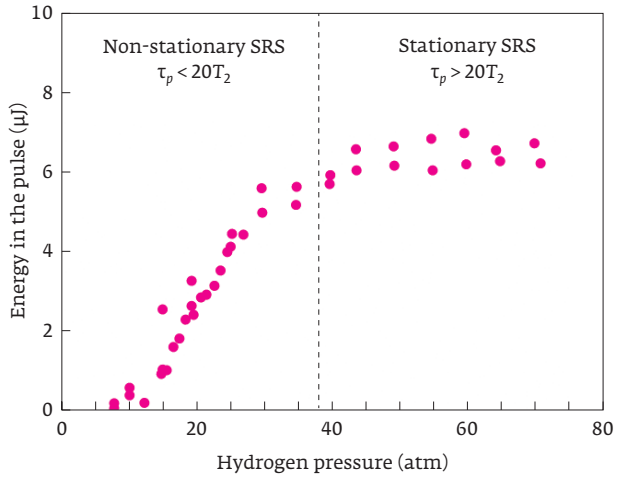

Fig. 13. *The experimental dependence of the pulse energy of the output radiation at a wavelength of 4.4 μm on the pressure of light hydrogen in the hollow core [59]. The duration of the pump pulses was $\tau_p = 3.5$ ns. The vertical dashed line corresponds to a pressure of 38 atm, at which the time of transverse relaxation of the molecular vibrations of hydrogen is $T_2 = 0.175$ ns, satisfying the relation $\tau_p = 20 \cdot T_2$.*

of the Raman laser (Fig. 13), which was pumped by pulses of duration τ_p=3.5 ns.

By optimizing the length of the fiber and the pressure of hydrogen in the hollow core, as well as using linearly polarized pump radiation at a wavelength of 1.56 μm and a Raman laser scheme that allows maintaining the polarization of radiation, a 53% quantum efficiency was achieved for a single-stage conversion of 1.56 → 4.42 μm. It was possible to demonstrate the SRS generation of nanosecond pulses at a wavelength of 4.4 μm with an average power of 1.4 W [64], while the rotational components at wavelengths of 1.72 and 1.91 μm were significantly suppressed. Fig. 14 shows the emission spectrum at the output of such a Raman laser and the dependences of the output power on the pump power obtained.

The currently demonstrated peak power of pulsed nanosecond gas fiber Raman lasers generating in the region of 3–5 μm is about 2 kW [59]. This value is limited not by the characteristics of the RF, but by the available power of the fiber erbium pump laser. Recent researches [65, 66] have demonstrated gas fiber Raman lasers with an output peak power of 400 kW and 150 kW at wavelengths of 1.55 and 1.9 microns, respectively. The use of such lasers as a pump source for gas-filled quartz RF opens the way to the creation of efficient gas fiber Raman lasers generating nanosecond pulses with a peak power of ~100 kW in the spectral range of 3–5 μm. Furthermore, such mid-IR lasers can be realized due to two-stage Raman scattering in the same section of the RF filled with one or more gases.

It is known that the Raman conversion from the near (λ = 1.56 μm) to the mid-IR range (λ = 3–5 μm) is accompanied by a large quantum defect, which can make it difficult to obtain a high average power at the Stokes wavelength. However, in a recent researcg [53]

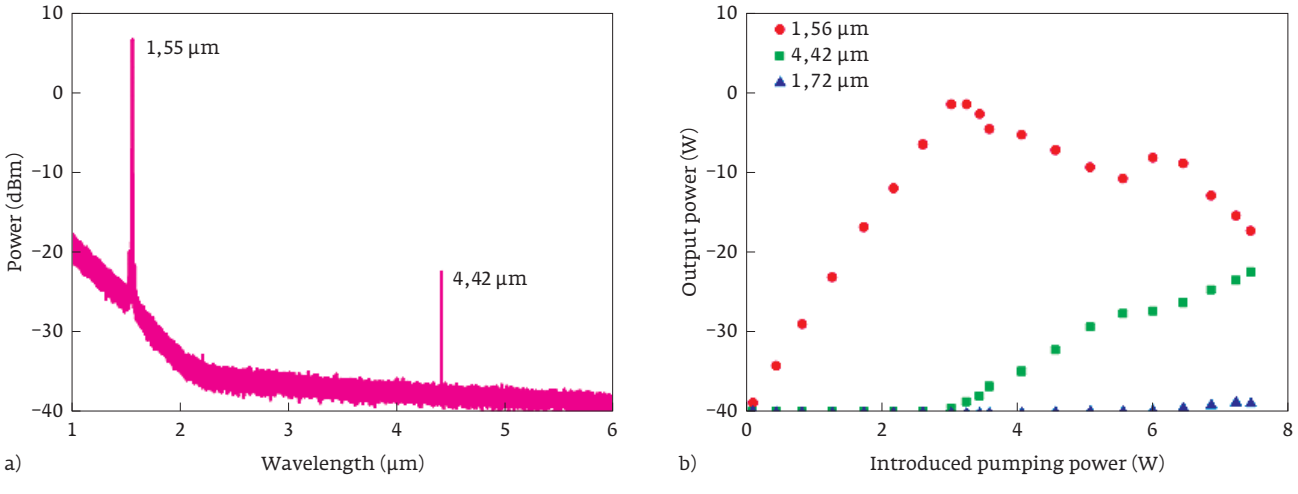

Fig. 14. *(a) characteristic emission spectrum at the output of a gas fiber Raman laser; (b) the dependence of the average power of the Raman laser on the average pumping power (1.56 μm) introduced into the fiber for the pumping, vibrational (4.42 μm), and rotational (1.72 μm) components of the Raman laser*

devoted to gas fiber lasers based on population inversion, efficient generation of radiation at a wavelength of 3.1 μm when pumped at λ = 1.53 μm was demonstrated. Despite a large quantum defect comparable to a quantum defect in Raman lasers, an output power of more than 1 W was achieved in a continuous mode. This result emphasizes the capabilities of gas fiber hollow-core fiber lasers, including Raman lasers, to generate high average power in the mid-IR range with a large quantum defect and the corresponding energy release in the fiber.

CONCLUSION

Compared to other hollow optical fibers, the RF are distinguished, first of all, by the simplicity of their design. Being made of quartz glass, they are capable of transporting radiation with wavelengths from vacuum ultraviolet to the mid-IR range. It was experimentally shown that the optical loss in the RF does not exceed a level of the order of 1 dB/m in the range from 200 nm to 4.4 μm. In the near IR region, hollow photonic crystal fibers (PCF) exhibit lower losses (of the order of 1 dB/km per 1.5 μm versus 30 dB/km in RF (see Fig. 3). But in a PCF with a hollow core, radiation interacts with several periods of the photonic crystal, which, on the one hand, allows one to obtain low optical losses, and on the other hand, leads to an increase in optical losses in the spectral regions where the fiber material has high losses. RF, especially with simple capillaries in the cladding (see Fig. 1 (a, b)) are characterized by much less overlapping the radiation distribution with the fiber material, which allows the RF to work in the region of high losses of the cladding material, therefore, the first effective Raman lasers operating in the mid-IR range (at a wavelength of 4.4 μm) were created based on quartz glass RF. The ability to transport short high-power laser pulses without distortion, which can be and has been already applied in the delivery of radiation from the laser to the point of consumption, is among the advantages. This is facilitated by their high radiation strength and low nonlinearity [67]. Further advancement in the mid-IR range is possible due to the transition to chalcogenide RF. The first experiments in this area showed the possibility of transporting CO_2 laser radiation up to 10.6 μm.

REFERENCE

1. **Pryamikov, A. D.; Biriukov, A. S.; Kosolapov, A. F.; Plotnichenko, V. G.; Semjonov, S. L.; Dianov, E. M.** Demonstration of a waveguide regime for a silica hollow-core microstructured optical fiber with a negative curvature of the core boundary in the spectral region > 3.5 μm. *Opt. Express*. 2011; *19*: 1441–1448. doi: https://doi.org/10.1364/OE.19.001441.
2. **Wang, Y. Y.; Couny, F.; Roberts, P. J.; Benabid, F.** Low loss broadband transmission in optimized core-shape Kagome Hollow-Core PCF. In *Lasers and Electro-Optics (CLEO) and Quantum Electronics and Laser Science Conference (QELS), 2010 Conference on (2010)*; Lasers and Electro-Optics (CLEO) and Quantum Electronics and Laser Science Conference (QELS): San Jose, CA, USA, 2010; p. CPDB4.
3. **Yu, F.; Wadsworth, W. J.; Knight, J. C.** Low loss silica hollow core fibers for 3–4 μ m spectral region. *Opt. Express*. 2012; *20*: 11153–11158. doi: https://doi.org/10.1364/OE.20.011153.
4. **Kolyadin, A. N.; Kosolapov, A. F.; Pryamikov, A. D.; Biriukov, A. S.; Plotnichenko, V. G.; Dianov, E. M.** Light transmission in negative curvature hollow core fiber in extremely high material loss region. *Opt. Express*. 2013; *21*: 9514–9519. doi: https://doi.org/10.1364/OE.21.009514.
5. **Gladyshev, A. V; Kolyadin, A. N.; Kosolapov, A. F.; Yatsenko, Y. P.; Pryamikov, A. D.; Biryukov, A. S.; Bufetov, I. A.; Dianov, E. M.** Efficient 1.9-μm Raman generation in a hydrogen-filled hollow-core fibre. *Quantum Electron*. 2015; *45*: 807–812. doi:10.1070/QE2015v045n09ABEH015881.
6. **Belardi, W.** Design and Properties of Hollow Antiresonant Fibers for the Visible and Near Infrared Spectral Range. *J. Light. Technol*. 2015; *33*: 4497–4503. doi:10.1109/JLT.2015.2477775.
7. **Kosolapov, A. F.; Alagashev, G. K.; Kolyadin, A. N.; Pryamikov, A. D.; Biryukov, A. S.; Bufetov, I. A.; Dianov, E. M.** Hollow-core revolver fibre with a reflecting cladding consisting of double capillaries. *Quantum Electron*. 2016; *46*: 10–14. doi:10.1070/QEL15972.
8. **Belardi, W.; Knight, J. C.** Hollow antiresonant fibers with reduced attenuation. *Opt. Lett*. 2014; *39*: 1853–1856. doi: https://doi.org/10.1364/OL.39.001853.
9. **Wei, C.; Weiblen, R.J.; Menyuk, C.R.; Hu, J.** Negative curvature fibers. *Adv. Opt. Photonics*. 2017; 9: 504–561
10. **Marcatili, E. A. J.; Schmeltzer, R. A.** Hollow Metallic and Dielectric Waveguides for Long Distance Optical Transmission and Lasers. *Bell Syst. Tech. J*. 1964; *43*: 1783–1809. doi:10.1002/j.1538–7305.1964.tb04108.x.
11. **Vajnshtejn, L. A.** *Elektromagnitnye volny*. – M.: AST. 1988.
12. **Miyagi, M.; Nishida, S.** Transmission

Characteristics of Dielectric Tube Leaky Waveguide. *IEEE Trans. Microw. Theory Tech.* 1980; *28*, 536–541. doi:10.1109/TMTT.1980.1130115.

13. **Litchinitser, N. M.; Abeeluck, A. K.; Headley, C.; Eggleton, B. J.** Antiresonant reflecting photonic crystal optical waveguides. *Opt. Lett.* 2002; *27*:1592–1594, doi: https://doi.org/10.1364/OL.27.001592.
14. **Zheltikov, A. M.** Colors of thin films, antiresonant phenomena in optical systems, and the limiting loss of modes in hollow optical waveguides. *Uspekhi Fiz. Nauk.* 2008; *178*: 619–629. doi:10.3367/UFNr.0178.200806d.0619.
15. **Kosolapov, A. F.; Pryamikov, A. D.; Biriukov, A. S.; Vladimir, S.; Astapovich, M. S.; Snopatin, G. E.; Plotnichenko, V. G.; Churbanov, M. F.; Dianov, E. M.** Demonstration of CO_2 -laser power delivery through chalcogenide-glass fiber with negative-curvature hollow core. *Opt. Express.* 2011; *19*: 9–14. doi: https://doi.org/10.1364/OE.19.025723.
16. **Vincetti, L.; Setti, V.** Flexible tube lattice fibers for terahertz applications. *Opt. Express.* 2013; *21*: 3388–3399. doi:10.1016/j.yofte.2012.09.008.
17. **Kitamura, R.; Pilon, L.; Jonasz, M.** Optical constants of silica glass from extreme ultraviolet to far infrared at near room temperature. *Appl. Opt.* 2007; *46*: 8118–8133. doi: https://doi.org/10.1364/AO.46.008118.
18. **Belli, F.; Abdolvand, A.; Chang, W.; Travers, J. C.; Russell, P. S. J.** Vacuum-ultraviolet to infrared supercontinuum in hydrogen-filled photonic crystal fiber. *Optica.* 2015; *2*: 292–300. doi: https://doi.org/10.1364/OPTICA.2.000292.
19. **Humbach, O.; Fabian, H.; Grzesik, U.; Haken, U.; Heitmann, W.** Analysis of OH absorption bands in synthetic silica. *J. Non. Cryst. Solids.* 1996; *203*: 19–26, doi:10.1016/0022–3093(96)00329–8.
20. **Tomashuk, A. L.; Golant, K. M.** Radiation-resistant and radiation-sensitive silica optical fibers. In *Proc. of SPIE*; Moscow, Russian Federation. 2000; p. 188.
21. **Kryukova, E. B.; Plotnichenko, V. G.; Dianov, E. M.** IR absorption spectra in high-purity silica glasses fabricated by different technologies. In *Proceedings of SPIE*; Moscow, Russian Federation, 2000; 4083: 71–80.
22. **Roberts, P.; Couny, F.; Sabert, H.; Mangan, B.; Williams, D.; Farr, L.; Mason, M.; Tomlinson, A.; Birks, T.; Knight, J.; St J Russell, P.** Ultimate low loss of hollow-core photonic crystal fibres. *Opt. Express.* 2005; *13*: 236–244, doi: https://doi.org/10.1364/OPEX.13.000236.
23. **Fini, J. M.; Nicholson, J. W.; Windeler, R. S.; Monberg, E. M.; Meng, L.; Mangan, B.; DeSantolo, A.; DiMarcello, F. V.** Low-loss hollow-core fibers with improved single-modedness. *Opt. Express.* 2013; *21*: 6233–6242. doi:10.1364/OE.21.006233.
24. **Wheeler, N.; Heidt, A.; Petrovich, M.; Baddela, N.; Numkam-fokoua, A.; Hayes, J.; Sandoghchi, S. R.; Poletti, F.; Wheeler, N. V.; Heidt, A. M.; Baddela, N. K.; Fokoua, E. N.; Hayes, J. R.; Sandoghchi, S. R.; Petrovich, M. N.; Richardson, D. J.** Low-loss and low-bend-sensitivity mid-infrared guidance in a hollow-core-photonic-bandgap fiber. *Opt. Lett.* 2014; *39*: 295–298. doi: https://doi.org/10.1364/OL.39.000295.
25. **Wang, Y. Y.; Wheeler, N. V; Couny, F.; Roberts, P. J.; Benabid, F.** Low loss broadband transmission in hypocycloid-core Kagome hollow-core photonic crystal fiber. *Opt. Lett.* 2011; *36*: 669–671. doi: https://doi.org/10.1364/OL.36.000669.
26. **Février, S.; Beaudou, B.; Viale, P.** Understanding origin of loss in large pitch hollow-core photonic crystal fibers and their design simplification. *Opt. Express.* 2010; *18*: 5142–5150. doi: https://doi.org/10.1364/OE.18.005142.
27. **Gérôme, F.; Jamier, R.; Auguste, J.-L.; Humbert, G.; Blondy, J.-M.** Simplified hollow-core photonic crystal fiber. *Opt. Lett.* 2010; *35*: 1157–1159. doi: https://doi.org/10.1364/OL.35.001157.
28. **Urich, A.; Maier, R. R. J.; Yu, F.; Knight, J. C.; Hand, D. P.; Shephard, J. D.** Flexible delivery of Er:YAG radiation at 2. 94 μm with negative curvature silica glass fibers: a new solution for minimally invasive surgical procedures. *Biomed. Opt. Express.* 2013; *4*: 7139–7144. doi: https://doi.org/10.1364/BOE.4.000193.
29. **Hartung, A.; Kobelke, J.; Schwuchow, A.; Wondraczek, K.; Bierlich, J.; Popp, J.; Frosch, T.; Schmidt, M. A.** Double antiresonant hollow core fiber – guidance in the deep ultraviolet by modified tunneling leaky modes. *Opt. Express.* 2014; *22*: 19131. doi:10.1364/OE.22.019131.
30. **Pryamikov, A. D.; Kosolapov, A. F.; Alagashev, G. K.; Kolyadin, A. N.; Vel'miskin, V. V; Biriukov, A. S.; Bufetov, I. A.** Hollow-core microstructured 'revolver' fibre for the UV spectral range. *Quantum Electron.* 2016; *46*: 1129–1133. doi:10.1070/QEL16227.
31. **Gladyshev, A. V; Kosolapov, A. F.; Kolyadin, A. N.; Astapovich, M. S.; Pryamikov, A. D.; Likhachev, M. E.; Bufetov, I. A.** Mid-IR hollow-core silica fibre Raman lasers. *Quantum Electron.* 2017; *47*:1078–1082. doi:10.1070/QEL16548.
32. **Wang, Z.; Belardi, W.; Yu, F.; Wadsworth, W.**

J.; Knight, J. C. Efficient diode-pumped mid-infrared emission from acetylene-filled hollow-core fiber. *Opt. Express*. 2014; *22*: 21872–8. doi:10.1364/OE.22.021872.

33. **Michieletto, M.; Lyngsø, J. K.; Jakobsen, C.; Lægsgaard, J.; Bang, O.; Alkeskjold, T. T.** Hollow-core fibers for high power pulse delivery. *Opt. Express*. 2016; *24*: 7103. doi:10.1364/OE.24.007103.
34. **Uebel, P.; Günendi, M. C.; Frosz, M. H.; Ahmed, G.; Edavalath, N. N.; Ménard, J.-M.; Russell, P. S. J.** Broadband robustly single-mode hollow-core PCF by resonant filtering of higher-order modes. *Opt. Lett*. 2016; *41*: 1961. doi:10.1364/OL.41.001961.
35. **Krylov, A. A.; Senatorov, A. K.; Pryamikov, A. D.; Kosolapov, A. F.; Kolyadin, A. N.; Alagashev, G. K.; Gladyshev, A. V.; Bufetov, I. A.** 1.56 μm Sub-Microjoule Femtosecond Pulse Delivery Through Low-Loss Microstructured Revolver Hollow-Core Fiber. *Laser Phys. Lett*. 2017; *14*: 035104. doi:10.1088/1612–202X/aa5a9b.
36. **Gauthier, J.-C.; Fortin, V.; Carrée, J.-Y.; Poulain, S.; Poulain, M.; Vallée, R.; Bernier, M.** Mid-IR supercontinuum from 2.4 to 5.4 μm in a low-loss fluoroindate fiber. *Opt. Lett*. 2016; *41*: 1756. doi:10.1364/ol.41.001756.
37. **Tang, Z.; Shiryaev, V. S.; Furniss, D.; Sojka, L.; Sujecki, S.; Benson, T. M.; Seddon, A. B.; Churbanov, M. F.** Low loss Ge-As-Se chalcogenide glass fiber, fabricated using extruded preform, for mid-infrared photonics. *Opt. Mater. Express* 2015; 5, 1722, doi:10.1364/OME.5.001722.
38. **Sanghera, J.; Aggarwal, I. D.** *Infrared Fiber Optics*; CRC Press: Boca Raton, FL, USA. 1998; ISBN9780849324895 – CAT# 2489.
39. **Artyushenko, V.; Bocharnikov, A.; Sakharova, T.; Usenov, I.** Mid-infrared Fiber Optics for 1–18 μm Range. *Opt. Photonik*. 2014; *9*: 35–39. doi:10.1002/opph.201400062.
40. **Hassan Muhammad Rosdi, A.; Yu, F.; J. Wadsworth, W.; Knight, J. C.** Cavity-based mid-IR fiber gas laser pumped by a diode laser. *Optica*. 2016; *3*: 218–221. doi:10.1364/OPTICA.3.000218.
41. **Wei, C.; Hu, J.; Menyuk, C. R.** Comparison of Loss in Silica and Chalcogenide Negative Curvature Fibers as the Wavelength Varies. *Front. Phys*. 2016; *4*: 1–10. doi:10.3389/fphy.2016.00030.
42. **Gladyshev, A. V; Kosolapov, A. F.; Khudyakov, M. M.; Yatsenko, Y. P.; Kolyadin, A. N.; Krylov, A. A.** 4. 4 μm Raman Laser Based on Hydrogen-Filled Hollow-Core Silica Fiber. In *Conference on Lasers and Electro-Optics*; San Jose, California United States. 2017; p. JTh5A.7.
43. **Gladyshev, A. V; Kosolapov, A. F.; Khudyakov, M. M.; Yatsenko, Y. P.; Kolyadin, A. N.; Krylov, A. A.; Pryamikov, A. D.; Biriukov, A. S.; Likhachev, M. E.; Bufetov, I. A.; Dianov, E. M.** 4.4-um Raman laser based on hollow-core silica fibre. *Quantum Electron*. 2017; *47*: 491–494. doi:10.1070/QEL16400.
44. **Gao, S.-F.; Wang, Y.-Y.; Ding, W.; Wang, P.** Hollow-core negative-curvature fiber for UV guidance. *Opt. Lett*. 2018; *43*: 1347. doi:10.1364/OL.43.001347.
45. **Denisov, A. N.; Kosolapov, A. F.; Senatorov, A. K.; Pal'tsev, P. E.; Semjonov, S. L.** Fabrication of microstructured optical fibres by drawing preforms sealed at their top end. *Quantum Electron*. 2016; *46*:1031–1039. doi:10.1070/QEL16212.
46. **Yakovlev, A. I.; Snetkov, I. L.; Dorofeev, V. V.; Motorin, S. E.** Magneto-optical properties of high-purity zinc-tellurite glasses. *J. Non. Cryst. Solids*. 2018; *480*: 90–94. doi:10.1016/j.jnoncrysol.2017.08.026.
47. **Shiryaev, V. S.; Kosolapov, A. F.; Pryamikov, A. D.; Snopatin, G. E.; Churbanov, M. F.; Biriukov, A. S.; Kotereva, T. V.; Mishinov, S. V.; Alagashev, G. K.; Kolyadin, A. N.** Development of technique for preparation of As2S3 glass preforms for hollow core microstructured optical fibers. *J. Optoelectron. Adv. Mater*. 2014; *16*: 1020–1025.
48. **Rafael R. Gattass, Daniel Rhonehouse, Daniel Gibson, Collin C. McClain, Rajesh Thapa, Vinh Q. Nguyen, Shyam S. Bayya, R. Joseph Weiblen, Curtis R. Menyuk, L. Brandon Shaw, and J. S. S.** Infrared glass-based negative-curvature anti-resonant fibers fabricated through extrusion. *Opt. Express*. 2016; *24*: 546–547. doi:10.1364/OE.24.025697.
49. **Gladyshev, A.; Kosolapov, A. F.; Khudyakov, M. M.; Yatsenko, Y. P.; Senatorov, A. K.; Kolyadin, A. N.; Krylov, A. A.; Plotnichenko, V. G.; Likhachev, M. E.; Bufetov, I. A.; Dianov, E. M.** Raman Generation in 2.9–3.5 μm Spectral Range in Revolver Hollow-Core Silica Fiber Filled by H_2/D_2 Mixture. In *Conference on Lasers and Electro-Optics*. 2017; p. STu1K.2.
50. **Benabid, F.; Knight, J. C.; Antonopoulos, G.; Russell, P. S. J.** Stimulated Raman scattering in hydrogen-filled hollow-core photonic crystal fiber. *Science*. 2002; *298*: 399–402. doi:10.1126/science.1076408.
51. **Wang, Z.; Yu, F.; Wadsworth, W. J.; Knight, J. C.** Efficient 1.9 μ m emission in H 2 -filled hollow core fiber by pure stimulated vibrational Raman scattering. *Laser Phys. Lett*. 2014; *11*, 105807,

doi:10.1088/1612–2011/11/10/105807.

52. **Benoit, A.; Beaudou, B.; Debord, B.; Gerome, F.; Benabid, F.**High power Raman-converter based on H 2 -filled inhibited coupling HC-PCF. In *Proc. SPIE10088*; San Francisco, California, United States. 2000; p. 100880H.
53. **Xu, M.; Yu, F.; Knight, J.** Mid-infrared 1 W hollow-core fiber gas laser source. *Opt. Lett.* 2017; *42*:4055. doi:10.1364/OL.42.004055.
54. **Couny, F.; Benabid, F.; Light, P. S.** Subwatt Threshold cw Raman Fiber-Gas Laser Based on H 2 -Filled Hollow-Core Photonic Crystal Fiber. *Phys. Rev. Lett.* 2007; *99*: 143903. doi:10.1103/PhysRevLett.99.143903.
55. **Bufetov, I. A; Dianov, E. M.** A simple analytic model of a cw multicascade fibre Raman laser. *Quantum Electron.* 2007; *30*, 873–877. doi:10.1070/QE2000v030n10ABEH001840.
56. **Miyagi, M.** Bending losses in hollow and dielectric tube leaky waveguides. *Appl. Opt.* 1981; *20*: 1221–1229. doi:10.1364/AO.20.001221.
57. **Kolyadin, A. N.; Astapovich, M. S.; Gladyshev, A. V; Kosolapov, A. F.** The Design Optimization and Experimental Investigation of the 4. 4 μm Raman Laser Basedon Hydrogen-filled Revolver Silica Fiber. In *VII International Conference on Photonics and Information Optics*; KnE Energy & Physics: Moscow, 2018; Vol. 2018: 47–64.
58. **Gladyshev, A. V; Kosolapov, A. F.; Khudyakov, M. M.; Yatsenko, Y. P.; Kolyadin, A. N.; Krylov, A. A.; Pryamikov, A. D.; Biriukov, A. S.; Likhachev, M. E.; Bufetov, I. A.; Dianov, E. M.** 2.9, 3.3, and 3.5 μm Raman Lasers Based on Revolver Hollow-Core Silica Fiber Filled by 1H2/D2 Gas Mixture. *IEEE J. Sel. Top. Quantum Electron.* 2018; *24*: 0903008, doi:10.1109/JSTQE.2018.2810378.
59. **Astapovich, M. S.; Kolyadin, A. N.; Gladyshev, A.; Kosolapov, A. F.; Pryamikov, A. D.; Khudyakov, M.; Likhachev, M. E.; Bufetov, I. A.** Efficient 4.4 μm Raman Laser Based on Hydrogen-Filled Hollow-Core Silica Fiber. *arXiv:1801.01729*.
60. **Gladyshev, A. V.; Kosolapov, A. F.; Astapovich, M. S.; Kolyadin, A. N.; Pryamikov, A. D.; Khudyakov, M. M.; Likhachev, M. E.; Bufetov, I. A.** Revolver Hollow-Core Fibers and Raman Fiber Lasers. *2018 Opt. Fiber Commun. Conf. Expo.* 2018, M2J.7. doi:10.1364/ofc.2018.m2j.7.
61. **Hanna, D. C.; Pointer, D. J.; Pratt, D. J.** Stimulated Raman Scattering of Picosecond Light Pulses in Hydrogen, Deuterium, and Methane. *IEEE J. Quantum Electron.* 1986; *22*: 332–336. doi:10.1109/JQE.1986.1072945.
62. **Weber, M. J.** CRC *Handbook of Laser Science and Technology Supplement 2: Optical Materials*. In; CRC Press. 1994; p. 334. ISBN9780849335075.
63. **Bischel, W. K.; Black, G.** Wavelength dependence of raman scattering cross sections from 200–600 nm. In *AIP Conference Proceedings*; American Institute of Physics, 1983; Vol. 100:181–187.
64. **Astapovich, M. S.; Gladyshev, A. V; Khudyakov, M. M.; Kosolapov, A. F.; Likhachev, M. E.; Bufetov, I. A.** 4.4-μm Raman generation with an average power above 1 W in silica revolver fibre. *Quantum Electron.* 2018; *48*:1084–1088. doi:10.1070/qel16836.
65. **Chen, Y.; Wang, Z.; Gu, B.; Yu, F.; Lu, Q.** Achieving a 1.5 $μ$m fiber gas Raman laser source with about 400 kW of peak power and a 6.3 GHz linewidth. *Opt. Lett.* 2016; *41*: 5118–5121. doi:10.1364/OL.41.005118.
66. **Wang, Z.; Gu, B.; Chen, Y.; Li, Z.; Xi, X.** Demonstration of a 150-kW-peak-power, 2-GHz-linewidth, 1.9-μm fiber gas Raman source. *Appl. Opt.* 2017; *56*: 7657–7661. doi:10.1364/AO.56.007657.
67. **Kolyadin A. N., Kosolapov A. F., Bufetov I. A.** Optical discharge propagation along hollow-core optical fibres. *Quantum Electron.* 2018; 48(12): 1138–1142.